Article:
Mehmood, F., Khan, B., Ali, S.M. et al. (2019) Distributed model predictive based secondary control for economic production and frequency regulation of microgrid. IET Control Theory and Applications, 13 (17). pp. 2948-2958. ISSN: 1751-8644

https://doi.org/10.1049/iet-cta.2018.6226

Distributed Model Predictive based Secondary Control for Economic Production and Frequency Regulation of Microgrid

F. Mehmood [1*], B. Khan [1], S. M. Ali [1], J. A. Rossiter[2]

[1] Department of Electrical Engineering, COMSATS University Islamabad, Abbottabad Campus, Pakistan.
[2] Department of Automatic Control and Systems Engineering, University of Sheffield, UK.
[*]faisalmehmood@ciit.net.pk

Abstract: This work focuses on Distributed Secondary Control (DSC) technique, for frequency regulation and Economic Load Dispatch (ELD) of Microgrid (MG). The fluctuating nature and large quantity of Distributed Energy Resources (DER) in autonomous MG result in complex control requirements, demanding fast and robust response. The contemporary DSC schemes are mostly based on Distributed Averaging Integration technique, owing slow response. The paper proposes, Distributed Model Predictive based Secondary Control (DMPSC) which effectively comply with the control requirements of MG. DMPSC requires each DER-node to solve a local optimization problem with the cost function penalizing the deviation of states from their desired values and difference between the assumed and predicted values. The desired-states for non-linear dynamics of DER-nodes, are based on local intermediate-optimum values, computed using local and neighbouring information. Equality based terminal constraints are introduced to ensure the stability, where each node is forced to reach the desired-state value at the end of prediction horizon. The terminal-consensus of the network affirms convergence of desired-states to a global optimal point of the network. The asymptotic stability of proposed control is proved by using the sum of local cost-functions as Lyapunov candidate function. Simulation results validate the effectiveness of the proposed control scheme.

1. Introduction

Expanding fraction of power generation by Distributed Energy Resources (DER) has given significant research importance to Microgrid (MG) [1]. MG is an accumulation of heterogenous sources (preferably DERs), storage device and load, beside possess the capability to operate in grid-connected and islanded mode. This flexibility of MG comes at the expense of control complexity. Small capacity, physically widely-distributed, large number and fluctuating output of DERs has resulted in several control challenges in MG, particularly related to the stability of the system [2]. Proportional-Integral based control solutions have been proposed in contemporary research to address the requirements of MG. Growing penetration of DERs with distinctive fluctuating nature is continuously demanding fast and robust control, especially for maintaining frequency (and voltage) stabilization and cost-efficient operation. This research work proposes a Distributed Model Predictive Control (DMPC) based solution, effectively complying with the control demands.

The power produced by DERs is in the form of DC (photovoltaic, fuel cells) or variable AC (wind turbine, microturbine) requiring a DC to AC inverter to inject the power in AC gird. Unlike synchronous generators, these inverter-interfaced DERs have inadequacy of fundamental synchronization mechanism due to absence of rotational inertial [3], [4]. It is clear from growing dependence on DERs that various control operations are to be achieved through control of inverters. The control objectives of MG consist of; balance of power, voltage and frequency regulation, sharing of load among the inverters, minimization of cost of production [5], [6], [7], [8] and phase synchronous with wide area gird [9], [10], [11].

The control required to achieve the above-mentioned control objectives is organized in hierarchical form, with each layer serving specific control objectives [12]. The Primary Control (first layer), uses decentralized droop control technique for active and reactive power sharing among the inverters. The proportional technique used in primary control causes deviation, from nominal values, in frequency and voltage. The Secondary Control (SC) (second layer) is used to keep the frequency and voltage at their nominal values. The Tertiary Control (third layer) provides the Economic Load Dispatch (ELD) to minimize the cost of production. However, the recent research has merged the Tertiary Control within the SC, providing the frequency regulation and ELD at the same level (SC level) [5], [6], [7], [8], [13]. The SC can be centralized [14], [15] as in conventional system, decentralized [16], [17], [18] as well as distributed [5], [19], [20], [21]. However, DSC has gained a lot of interest recently providing eased plug and play to expanding number of DERs.

In Centralized Secondary Control the central control unit is connected with all the generating units through communication links. Conventionally, centralized control contains PI based Automatic Generation Control that makes use of Area Control Error to regulate the frequency and power flow between different Areas [22]. Similarly, at MG level, Microgrid Central Control (MGCC) is used that makes use of low bandwidth communication channels with DERs [14], [15]. The centralized control architecture, however, is not a preferred choice, specifically in the presence of a large quantity of small-scale DERs [23], also the communication link failure with DER node/nodes, may intimidate the frequency regulation of the system. The Decentralized Secondary Control uses local control at each DER node [13] without any coordination with central control or peers. The integral based decentralized control may possess additional

equilibrium point and may fail to provide the optimum power injection profiles [5] and also, under adverse conditions may even fail to achieve the frequency regulation [24].

The DSC on the other hand, offers flexibility of eased plug and play, requiring only the communication with neighbouring DER node/nodes. DSC is unaffected by single link failure as long as DER nodes form a connected communication graph. Distributed Averaging Integrator based DSCs have been proposed in [24], [25], [26], where the control input of each node is based on neighbouring information and local frequency deviation. However, DAI based DSC possesses slow convergence, which is often compensated with larger gains, resulting in overshoot and oscillation problem. In the presence of fluctuating nature of DERs, fast convergence of SC is critical [6]. Other DSC schemes include, MPC and Smith Predictor based SC [27], provides the frequency regulation, but fails to assign optimum power injections to each node. A mixture of centralized and distributed control is used in [6] and [23]. The author, in [6] proposed Power Imbalance Allocation Control (PIAC), uses a PI based local control for frequency regulation and a centralized control within the Area to solve the optimization problem for ELD and Inter-Area power exchange. While, an integral based centralized control is proposed in [23] that aggregates the measured frequencies and broadcasts a control message to individual nodes, which uniquely interprets it based on local parameters.

Another control challenge of MG, switching between islanded and grid-connected mode is the phase synchronization. MG while operating in islanded mode, may deviate in phase angle from the main utility grid. The prerequisite of MG switching, from islanded to grid-connected mode, is the phase synchronization. The phase difference between MG and wide area grid should be within the acceptable limits at Point of Common Coupling (PCC) [11]. The phase synchronization issue has been dealt separately and has not been addressed in presented control hierarchy.

This paper focuses on the implementation of MPC technique at SC level. Traditionally, MPC is designed for a single agent system, where optimum control is achieved by solving the finite horizon optimal control problem. MPC has practically been utilized as centralized control, where all the states are known. However, in multiagent systems the centralized implementation is not suitable because of difficulties in collecting the information from physically distributed nodes and computation of large-scale optimization problem. DMPC has been introduced in [28], [29] for multiagent systems, relaxing the requirement of centralized control. Here, each node solves local optimal control problem based on information from its neighbouring peer nodes, so the size of the network does not affect the computational efficiency and performance of the control.

A Distributed Model Predictive based Secondary Control (DMPSC) is introduced in this paper for frequency regulation and ELD. DMPC with its inherent constraint handling capability, provides fast convergence as compared with integral based SC schemes. DMPSC efficiently provides the frequency regulation while maintaining the optimum power injection profile at each node. Based on local and neighbouring information, each DER node computes an intermediate-optimum phase angle and tracks the local phase towards that optimum phase direction, in each iteration. The significant contributions of the paper are highlighted below

- A model predictive based SC is proposed in this paper. The control is implemented in a distributed manner, each node communicates its information with neighbouring nodes, solves a local optimization problem and achieves the consensus asymptotically.
- Provides frequency regulation by maintaining the real power balance in the network and ELD, using identical cost criteria [5].
- Phase synchronization with wide-area is achieved by forcing a single node to follow the reference instantaneous phase. This is the foremost attempt to provide the phase synchronization in DSC.
- The sufficient condition for convergence of proposed control is derived and used the total cost of network as a Lyapunov candidate function to prove the Asymptotic stability of the system.
- Effectiveness of proposed control schemes is demonstrated with the help of MATLAB model and the results are compared with the DAI based control scheme.

The rest of the paper is organized as follows; Section 2, contains modelling of MG system and the control objects. The Section starts with introduction of notations used in the paper and graph theory, followed by dynamics of power network, explanation of control objectives and introduction of DAI control scheme. Section 3, introduces the proposed DMPSC algorithm, used as local control at each power-node. The stability analysis is presented in Section 4, consisting of convergence of desired-states to global optimum and convergence of the cost function. Lastly, Section 5, contains MATLAB based simulation results and comparison with DAI control**.**

2. Microgrid Modelling and Control Objectives

2.1 Notations

Let, the set of all real numbers be represented by $\mathbb{R}$, $\mathbb{C}$ represents the set of complex numbers and $\mathbb{O}$ represents the null set. $\mathbb{R}_{>0}$ denotes the set $\{x \in \mathbb{R} | x > 0\}$, $\mathbb{R}_{\geq 0}$ denotes the set $\{x \in \mathbb{R} | x \geq 0\}$, $\mathbb{R}_{<0}$ denotes the set $\{x \in \mathbb{R} | x < 0\}$ and $\mathbb{R}_{\leq 0}$ denotes the set $\{x \in \mathbb{R} | x \leq 0\}$. If S represents a set, then $|S|$ represents the cardinality of set S. $x \coloneqq colm(S), x \in \mathbb{R}^{|S|\times 1}$, represents a column vector of length $|S|$ and $X \coloneqq \mathfrak{D}(x) \in \mathbb{R}^{|S|\times|S|}$, represents a diagonal matrix containing all zeros except the diagonal entries containing x. $\mathbb{1}_n \in \mathbb{R}^{n\times 1}$, denotes a column vector of ones with length n and identity matrix is denoted by $I_n \in \mathbb{R}^{n\times n}$. For sets S_1 and S_2, $S_{1\cap 2}$ denotes $S_1 \cap S_2$ and S_{1-2} denotes $S_1 - S_2$. The operator " $\circ$ ", represents Hadamard product (elementwise multiplication) of matrices of same dimensions.

2.2 Graph Theory

Let $\mathbb{G}$, be a static, connected and undirected graph of n nodes, represented by the set $N = \{1, \dots n\}$. The nodes of $\mathbb{G}$, are connected through the edges, represented by $E \subseteq N \times N$

and $A \in \mathbb{R}^{n\times n}$ is the associated adjacency matrix ($A = A^T$) with elements $a_{ij} = 1$, $i,j \in N$, if the nodes i and j are connected by an edge and $a_{ij} = 0$, otherwise. The degree matrix of A, is denoted by $\mathbb{Q}_A \coloneqq \mathfrak{D}(d_{Ai}) \in \mathbb{R}^{n\times n}$, where d_{Ai}, is the i^{th} row-sum of A. The set of neighbouring nodes of i^{th} node is represented by $N_i \coloneqq \{n_j\}$, such that $a_{ij} = 1$, $i,j \in N$, ($d_{Ai} = |N_i|$). Let $\mathcal{L}_A \coloneqq \mathbb{Q}_A - A, \in \mathbb{R}^{n\times n}$, represented the associated Laplacian matrix of $\mathbb{G}$.

2.3 Power Network

Consider a power network consisting of a set of nodes; N ($n = |N|$) and represented by graph $\mathbb{G}$. The nodes in $\mathbb{G}$, are categorized as power-nodes and load-nodes. Power-nodes have a (renewable) power source and may contain a localized load as well. While, load-node are the ones that (only) consume the real power. Both types of nodes are respectively represented by $N_P = \{1, \dots n_P\}$ and $N_L = \{n_P + 1, \dots n_P + n_L\}$, such that $n = n_P + n_L$ ($\mathrm{N} = N_P \cup N_L$).

The power consumption by i^{th} load-node is represented by $p_{l,i}$. The power network forms a connected graph in terms of power lines, that is, there exist a path (of power-lines) between all possible pairs of nodes in N. For simplicity, the power lines are assumed to be lossless (pure inductive lines). The set $N_{bP,i}$, represents the neighbouring power-nodes, while $N_{bL,i}$, represents the neighbouring load-nodes, of i^{th} node. The matrix $B_P \in \mathbb{R}^{n_P\times n_P}$, (with elements; $b_{P,ij}$) represents the susceptance matrix between the power-nodes, while $B_L \in \mathbb{R}^{n_p\times n_L}$, (with elements; $b_{L,ij}$) represents the susceptance matrix between power and load nodes. The adjacency matrices corresponding to B_P is represented by $A_{bP}, \in \mathbb{R}^{n_P\times n_P}$. The power-nodes also form a connected sub-graph in terms of communication links. The set of neighbouring communication nodes of i^{th} node is represented by $N_{c,i}$ with corresponding adjacency matrix represented by $A_c, \in \mathbb{R}^{n_P\times n_P}$. The degree matrices of B_P, B_L, B_L^T and A_c are denoted by $\mathbb{Q}_{bP}, \in \mathbb{R}^{n_P\times n_P}$, $\mathbb{Q}_{bL}, \in \mathbb{R}^{n_P\times n_P}$, $\mathbb{Q}_{bL}^{\perp}, \in \mathbb{R}^{n_L\times n_L}$ and $\mathbb{Q}_c, \in \mathbb{R}^{n_P\times n_P}$, ($\mathbb{Q}_{bL} = \mathfrak{D}\big(B_L \mathbb{1}_{n_L}\big)$ and $\mathbb{Q}_{bL}^{\perp} = \mathfrak{D}\big(B_L^T \mathbb{1}_{n_P}\big)$). The instantaneous phase angle and voltage magnitude of each power node is represented by θ_i, and v_i, respectively. For simplicity the voltage magnitude at each node is considered as 1p.u.

Emulating the behaviour of synchronous generator [26], the discretised dynamics of power-node is given in (1).

Where, Δt is the sampling time, t represents the discrete time, $\theta_i(t)$ and $\omega_i(t)$ represent the phase and angular frequency of i^{th} inverter. $d_i \in \mathbb{R}_{>0}$ is the damping coefficient, $m_i \in \mathbb{R}_{>0}$ is the virtual inertia of inverter [16], [17]. $\omega_d \in \mathbb{R}_{>0}$ is the desired angular frequency of the system. $f_i \in \mathbb{R}$ is the additional state, represents the integrated control effort, while $\tau \in \mathbb{R}_{>0}$ represents the inertial lag and $u_i \in \mathbb{R}$ is the control input. p_i is the total power production of i^{th} node, contains of power flow to the neighbouring power-nodes and load,

$$p_i(t) = \sum_{j\in N_{bP,i}} \Big(b_{P,ij} v_i v_j \sin\Big(\theta_i(t) - \theta_j(t)\Big)\Big) + p_i^L(t), \quad (2)$$

p_i^L denotes the power delivered to the load; $p_i^L(t) = p_{LL,i} + p_{L,i}(t)$, where $p_{LL,i}$ represents the local power consumption of power-node, while $p_{L,i}(t)$ represents the power delivered to load-nodes

$$p_{LL,i} = \frac{|v_i|^2}{R_{LLi}}, \quad i \in N_P, \quad (3)$$

$$p_{L,i}(t) = \sum_{j\in N_{bL,i}} \Big(b_{L,ij} v_i v_j \sin\Big(\theta_i(t) - \theta_j(t)\Big)\Big), \quad i \in N_P, \quad (4)$$

Where, $R_{LL,i}$ is the resistance of local load. To translate the dynamic equations in terms of deviation variable, let $\Delta\omega_i(t) = \omega_i(t) - \omega_d$ and $\Delta\theta_i(t) = \theta_i(t) - \theta_d(t)$, where $\theta_d(t) = k\omega_d\Delta t$ and discrete variable $k = {}^{t}/_{\Delta t} = 0, 1, 2, \dots$. (or $t = k\Delta t$). For above translation, $\Delta\theta_i(t) - \Delta\theta_j(t) = \theta_i(t) - \theta_j(t)$, also subtracting ω_d from both side of (1) results in; $\Delta f_i(t) = f_i(t)$. So (1) can be rewritten as (5).

Let, the states of the system be represented by $\chi_i = [\Delta\theta_i \quad \Delta\omega_i \quad \Delta f_i]^T \in \mathbb{R}^{3\times 1}$, and $y_i = [\Delta\theta_i \quad \Delta\omega_i]^T \in \mathbb{R}^{2\times 1}$ denote the output vector. Further (5) can be compactly represented as,

$$\begin{aligned} \chi_i(t+1) &= \mathcal{F}\Big(\chi_i(t), \Delta\theta_j(t), u_i(t)\Big), \\ & i \in N_P, j \in N_{bP,i} \cup N_{bL,i}, \\ y_i(t) &= \Theta\chi_i(t), \qquad i \in N_P, \end{aligned}$$

the Θ and $\mathcal{F}(.)$ are defined in (6) and (7).

$$\begin{aligned} \theta_i(t+1) &= \theta_i(t) + \omega_i(t)\Delta t, \\ \omega_i(t+1) &= \omega_i(t) + \tfrac{\Delta t}{m_i}[-d_i(\omega_i(t) - \omega_d) - p_i(t) + f_i(t)], \\ f_i(t+1) &= f_i(t) - \tfrac{\Delta t}{\tau} f_i(t)_i + \tfrac{\Delta t}{\tau} u_i(t), \end{aligned} \quad (1)$$

$$\begin{aligned} \Delta\theta_i(t+1) &= \Delta\theta_i(t) + \Delta\omega_i(t)\Delta t, \\ \Delta\omega_i(t+1) &= \Delta\omega_i(t) + \tfrac{\Delta t}{m_i}\Big[-d_i\Delta\omega_i(t) - \textstyle\sum_{j\in N_{bP,i}}\Big(b_{P,ij} v_i v_j \sin\Big(\Delta\theta_i(t) - \Delta\theta_j(t)\Big)\Big) - \\ &\qquad \textstyle\sum_{j\in N_{bL,i}}\Big(b_{L,ij} v_i v_j \sin\Big(\Delta\theta_i(t) - \Delta\theta_j(t)\Big)\Big) - \tfrac{|v_i|^2}{R_{LLi}} + \Delta f_i(t)\Big], \\ \Delta f_i(t+1) &= \Delta f_i(t) - \tfrac{\Delta t}{\tau}\Delta f_i(t)_i + \tfrac{\Delta t}{\tau} u_i(t), \end{aligned} \quad (5)$$

$$\Theta = \begin{bmatrix} 1 & 0 & 0 \\ 0 & 1 & 0 \end{bmatrix} \in \mathbb{R}^{2\times 3}, \quad (6)$$

$$\mathcal{F}\Big(\chi_i(t), \Delta\theta_j(t), u_i(t)\Big) = \chi_i(t) + \Delta t \begin{bmatrix} \Delta\omega_i(t) \\ \frac{1}{m_i}[-d_i\Delta\omega_i(t) - p_i(t) + \Delta f_i(t)] \\ -\frac{1}{\tau}\Delta f_i(t) + \frac{1}{\tau} u_i(t) \end{bmatrix}, \quad (7)$$

Assumption 1: We relax the condition of identical power and communication neighbours; $N_{ci} = N_{bPi}$. Instead, we assume that $N_{ci} \cap N_{bPi} \neq \mathbb{O}, i \in N_P$.

2.4 Objectives of Secondary Control

The objective of secondary control is to regulate the frequency to nominal values and minimize the cost of production. For cost minimization, optimum power production for each node is obtained from identical cost criteria introduced in [5]. So, the control objectives are;

$$\Delta\omega_i(t) = 0, \qquad i \in N_P. \tag{8}$$

$$\sum_{j\in N_P}\left(c_i p_i(t) - c_j p_j(t)\right) = 0, \qquad i \in N_P. \tag{9}$$

Where, c_i represents the incremental cost of power-nodes. Frequency regulation, the primary objective of SC is represented in (8), while (9) represents ELD objective and is based on identical marginal cost criteria for all power-nodes.

2.5 Distributed Averaging Integrator

The DAI control scheme is based on integration of errors in (8) and (9). The control law for DAI is represented in discrete form in (10).

Where, k_w and k_p are the tuning variables. The frequency deviation ($\Delta\omega_i(t)$) can be locally measured, in fact its value can be easily extracted from Primary Control of the inverter. Since, an i^{th} node cannot obtain the value of $p_j(t)$ from all the nodes in the network, it uses its communication neighbouring set $(N_{c,i})$ to form the error in (9). The control rapidly regulates the frequency to its nominal values but possesses slow converges to identical cost. Also, increasing k_p to improve ELD, adversely affects the frequency regulation, indicating its troublesome tuning.

3. Design of Distributed Model Predictive Secondary Control

Let $\chi_i^* = [\Delta\theta_i^*(t) \quad \Delta\omega_i^*(t) \quad \Delta f_i^*(t)]$, be the equilibrium point that globally satisfies the control objective (8) and (9). From (8), the equilibrium point for frequency deviation is; $\Delta\omega^* = 0$. Now, using the nearest neighbor communication approach of (10), (9) can be rewritten in matrix form as,

$$\mathcal{L}_c CP = 0. \tag{11}$$

Where $C = \mathfrak{D}(c_i) \in \mathbb{R}^{n_P\times n_P}$, $P = colm(p_i), \in \mathbb{R}^{n_P\times 1}$ and $\mathcal{L}_c = \mathbb{Q}_c - A_c \in \mathbb{R}^{n_P\times n_P}$ is the Laplacian matrix with rank equal to $n_P - 1$. So, the equilibrium points for $\Delta\theta_i$ and Δf_i cannot be obtained using (11). Since the equilibrium point is not known exactly, we adopt iterative method and find the desired-states ($\chi_i^d(t)$) in each iteration and force the state $\chi_i(t)$ to track the desired-state. The desired values are calculated based on local and neighbouring information and updated after each iteration, such that, $\chi_i^d(t)$ asymptotically converges to χ_i^* as $t \to \infty$. The desired-states are defined as,

$$\begin{aligned}\chi_i^d(t) &= [\Delta\theta_i^d(t) \quad \Delta\omega_i^d(t) \quad \Delta f_i^d(t)]^T \\ &= \Xi\left(\chi_i(t) + \alpha\left(\tilde{\chi}_i^*(t) - \chi_i(t)\right)\right), \quad i \in N_P\end{aligned}$$

Where, $\tilde{\chi}_i^*(t)$ is the local intermediate-optimum point that satisfies (8) and (9) at every discrete time t, $\alpha \coloneqq \{\alpha \in \mathbb{R} | 0 < \alpha < 1\}$ is the step size and $\Xi = \begin{bmatrix}1 & 0 & 0\\ 0 & 0 & 0\\ 0 & 0 & 1\end{bmatrix}$, implying that $\Delta\omega_i^d(t) = 0$ (also $\Delta\omega_i^d(t) = \Delta\tilde{\omega}_i^*(t) = 0$). Now using $\Delta\omega_i(t) = 0$, in (5) results in; $p_i(t) = \Delta f_i(t)$, (and during steady state; $p_i(t) = \Delta f_i(t) = u_i(t)$). Following the same approach of (10) and writing (9) using communication neighbouring set $(N_{c,i})$ provides; $\sum_{j\in N_{c,i}}\left(c_i p_i(t) - c_j p_j(t)\right) = 0$. So the value of intermediate-optimum power is,

$$\Delta\tilde{f}_i^*(t) = \tilde{p}_i^*(t) = \frac{\sum_{j\in N_{c,i}} c_j p_j(t)}{|N_{c,i}| c_i}, \quad i \in N_P \tag{12}$$

Note, that the value $\Delta\tilde{f}_i^*(t)$ is based entirely on neighbouring information and represents the intermediate-optimum power injection of local node. Now, to derive the value of $\Delta\tilde{\theta}_i^*(t)$, we evaluate (5) using (2), (8) and (12), and using Assumption 1, resulting in (13), (14) and (15).

Where $\acute{p}(t) = \sum_{j\in N_{bP-c,i}}\left(b_{P,ij} v_i v_j \sin\left(\Delta\theta_i(t) - \Delta\theta_j(t)\right)\right)$. The first two terms on right hand side, in (15), can be measured locally, while the last term is obtained using peer communication. We use the non-empty set $N_{bP\cap c,i}$ (Assumption 1) in (15) to find the intermediate phase equilibrium value.

Remark 1: The MG may shift from islanded to gird-connected mode, requiring a prior phase synchronization between MG and main grid [9], [10]. For that reason, the phase of a power-node near PCC (let it be node 1; n_1) is made to follow a reference value, such that phase difference at PCC is kept within the acceptable limits [12].

Without loss of generality, let the reference phase be $\theta_d(t) = k\omega_d\Delta t$ (used in (5)). So, from (15) we can obtain the value of $\Delta\tilde{\theta}_i^*(t)$ as presented in (16).

$$u(t+1) = u(t) - k_w\left(\Delta\omega_i(t)\right)\Delta t - k_p\sum_{j\in N_{c,i}}(c_i u_i(t) - c_j u_j(t))\Delta t, \tag{10}$$

$$\sum_{j\in N_{bP,i}}\left(b_{P,ij} v_i v_j \sin\left(\Delta\tilde{\theta}_i^*(t) - \Delta\theta_j(t)\right)\right) + p_i^L(t) = \Delta\tilde{f}_i^*(t), \tag{13}$$

$$\sum_{j\in N_{bP\cap c,i}}\left(b_{P,ij} v_i v_j \sin\left(\Delta\tilde{\theta}_i^*(t) - \Delta\theta_j(t)\right)\right) = -\sum_{j\in N_{bP-c,i}}\left(b_{P,ij} v_i v_j \sin\left(\Delta\theta_i(t) - \Delta\theta_j(t)\right)\right) - p_i^L(t) + \Delta\tilde{f}_i^*(t), \tag{14}$$

$$\sum_{j\in N_{bP\cap c,i}}\left(b_{P,ij} v_i v_j \sin\left(\Delta\tilde{\theta}_i^*(t) - \Delta\theta_j(t)\right)\right) = -\acute{p_i}(t) - p_i^L(t) + \Delta\tilde{f}_i^*(t), \tag{15}$$

$$\Delta\tilde{\theta}_i^*(t) = \begin{cases} 0, & i = 1, \\ sin^{-1}\left\{\frac{\acute{p_i}(t) - p_i^L(t) + f_i^d(t)}{\sqrt{\Upsilon_i(t)^2 + \wp_i(t)^2}}\right\} - tan^{-1}\left(\frac{\wp_i(t)}{\Upsilon_i(t)}\right), & i = 2 \dots n_P. \end{cases} \tag{16}$$

Where, $\Upsilon_i(t) = \sum_{j\in N_{bP\cap c,i}} b_{P,ij} v_i v_j \cos\left(\Delta\theta_j(t)\right)$ and $\wp_i(t) = \sum_{j\in N_{bP\cap c,i}} b_{P,ij} v_i v_j \sin\left(\Delta\theta_j(t)\right)$. From (12) and (16),

$$\chi_i^d(t) = \Xi(1-\alpha)\chi_i(t) + \Xi\alpha[\Delta\tilde{\theta}_i^*(t) \quad \Delta\tilde{\omega}_i^*(t) \quad \Delta\tilde{f}_i^*(t)],$$
$$y_i^d(t) = \Theta\chi_i^d(t) \tag{17}$$

3.1 Local Control of Power-Nodes

The local control of each node is designed to track the desired-state $\chi_i^d(t)$. The desired-state is calculated for compete length of prediction horizon ($\mathcal{N}_\wp$), with the help of local measurement and information from neighbouring nodes ($N_{c,i}$). The length of prediction horizon ($\mathcal{N}_\wp$), is same for all the individual power-nodes. Following [28][29], we define three different types of state trajectories over prediction horizon; $\chi_i^p(k|t)$, the predicted trajectories, $\chi_i^{op}(k|t)$, the optimal trajectories and $\chi_i^a(k|t)$, the assumed trajectories. The state trajectories $\chi_i^p(k|t)$ are used in the optimization problem, $\chi_i^{op}(k|t)$ is the optimal state trajectories obtained after solving the local optimization problem, while $\chi_i^a(k|t)$ is obtained from optimal trajectories by shifting one step in time. The assumed state trajectories are communicated between the neighbouring nodes to form the local control problem. Similarly, $u_i^p(k|t)$ denotes predicted control-input used in optimization problem while, $u_i^{op}(k|t)$ and $u_i^a(k|t)$ are the optimal control and assumed control input, respectively.

3.2 Optimization Problem $\mathbb{F}_i$

The local open-loop optimal control problem for i^{th} node is given below. The cost function penalizes the deviation of output from desired and assumed value.

$$min_{(u_i^p)}\ J_i\left(y_i^p(k|t), u_i^p(k|t), y_i^a(k|t), y_i^d(:|t)\right),$$
$$subj\ to.$$
$$\chi_i^p(0|t) = \chi_i^a(0|t),$$
$$\chi_i^p(k+1|t) = \mathcal{F}\left(x_i^p(k|t), \theta_j^a(k|t), u_i(k|t)\right),$$
$$y_i^p(k|t) = \Theta\chi_i^p(k|t),$$
$$u_i^p(k|t) \in U_i,$$
$$y_i^p\left(\mathcal{N}_\wp|t\right) = y_i^d\left(\mathcal{N}_\wp|t\right), \tag{18}$$
$$f_i^p\left(\mathcal{N}_\wp|t\right) = \Delta f_i^d\left(\mathcal{N}_\wp|t\right). \tag{19}$$

The cost function $J_i(.)$ is defined in (20). The terminal constraints (18) and (19), are used to force the state to reach the desired value; $\chi_i^d\left(\mathcal{N}_\wp|t\right)$, at the end of prediction horizon. $R \in \mathbb{R}_{>0}^{2\times2}$ and $S \in \mathbb{R}_{>0}^{2\times2}$ represents the symmetric weighting matrices. R penalizes the deviation of trajectories from desired values, while S penalizes the deviation between the assumed and predictive trajectories.

Remark 2: Tracking the desired value is actually tracking the local intermediate-optimum values at any given (discrete) time instant k. The desired value defined in (17) do not necessarily converge to a global optimum point and requires a careful selection of step size α. The sufficient condition for selection of α is discussed in Section 4.

3.3 DMPC Algorithm

The DMPSC algorithm consists of the following steps;

I. Initialization

$$\chi_i^a(0|0) = \chi_i(0) = \chi_{o,i},$$
$$u_i^a(:|0) = u_{o,i},$$

Communicate the initial state; $\chi_{o,i}$ to neighbouring nodes and construct the initial assumed values ($\chi_i^a(:|0)$),

$$\chi_i^a(k+1|0) = \mathcal{F}\left(\chi_i^a(k|0), \Delta\theta_j^a(0|0), u_i(k|0)\right),$$
$$y_i^a(k|0) = \Theta\chi_i^a(k|0), \quad k = 0,1,\dots,\mathcal{N}_\wp - 1,$$

II. DMPSC Iterations

1) Calculate the desired-states phase $\left(\chi_i^d(:|t)\right)$,
2) Solve the optimization problem $\mathbb{F}_i$, for optimum control input $u_i^{op}(:|t)$,
3) Compute the optimal trajectories,

$$\chi_i^{op}(0) = \chi_i(t),$$
$$\chi_i^{op}(k+1|t) = \mathcal{F}\left(\chi_i^{op}(k|t), \Delta\theta_j^a(k|t), u_i^{op}(k|t)\right),$$
$$k = 0,1,\dots,\mathcal{N}_\wp - 1,$$

4) Assumed values are obtained by one step shifting the optimum values,

$$u_i^a(k|t+1) = u_i^{op}(k+1|t), \quad k = 0,1,\dots,\mathcal{N}_\wp - 2,$$
$$\chi_i^a(k|t+1) = \chi_i^{op}(k+1|t) \quad k = 0,1,\dots,\mathcal{N}_\wp - 1, \tag{21}$$

5) The last value of assumed input maintains the desired-states as shown in (22) while, (23) represents the last value of assumed states.

1) Implement the first value of control law,
$\chi(t+1) = \mathcal{F}\left(\chi(t), \Delta\theta_j^a(0|t), u_i^{op}(0|t)\right)$,
2) Increment the time $t = t+1$,
3) Communicate the assumed values ($\chi_i^a(:|t)$, power injection $\left(p_i(t)\right)$ and incremental cost $\left(c_i(:|t)\right)$ to neighbouring nodes,
4) Go to step 1.

Where, $\chi_{o,i}$ and $u_{o,i}$ represent the initial values of states and input respectively. The state trajectories are forced to reach the desired values at the end of prediction horizon. Also, the last values of assumed input in (22) maintains the desired-state values achieved in (18) and (19). Step No. 6

$$J_i\left(y_i^p(k|t), u_i^p(k|t), y_i^a(k|t), y_i^d(k|t)\right) = \sum_{k=0}^{\mathcal{N}_\wp-1} \mathbb{l}_i\left(y_i^p(k|t), u_i^p(k|t), y_i^a(k|t), y_i^d(k|t)\right),$$
$$= \sum_{k=0}^{\mathcal{N}_\wp-1} ||y_i^p(k|t) - y_i^d(k|t)||_R + ||y_i^p(k|t) - y_i^a(k|t)||_S, \tag{20}$$

$$u_i^a\left(\mathcal{N}_\wp - 1|t+1\right) = \Delta f_i^d\left(\mathcal{N}_\wp|t\right), \tag{22}$$

$$\chi_i^a\left(\mathcal{N}_\wp|t+1\right) = \mathcal{F}\left(\chi_i^a\left(\mathcal{N}_\wp - 1|t+1\right), \Delta\theta_j^a\left(\mathcal{N}_\wp - 1|t\right), u_i^a\left(\mathcal{N}_\wp - 1|t+1\right)\right),$$
$$y_i^a(k|t+1) = \Theta\chi_i^a(k|t+1), \tag{23}$$

implements the first value of control input to update the actual states. In Step No. 1, the desired values are calculated using the (local and neighbouring) assumed states trajectories, over the complete length of prediction horizon. Equation (17) involves intermediate-optimum state trajectories ($\tilde{\chi}_i^*(:|t)$), for which $\Delta\tilde{f}_i^*(:|t)$ is calculated using (12) $\left(\Delta\tilde{f}_i^*(:|t) = \Delta\tilde{f}_i^*(t)\right)$ and $\Delta\tilde{\theta}_i^*(:|t)$ is obtained using (16) (employing $\Delta\theta_j^a(:|t)$, $p_\iota\acute{}(t)$ and $p_i^L(t)$). Note that the value of $\Delta\tilde{f}_i^*(:|t)$, $p_\iota\acute{}(t)$ and $p_i^L(t)$ do not change over prediction horizon.

4. Stability Analysis

This Section discusses the stability of DMPSC algorithm. The stability is discussed in two portions, first the convergence of desired-states to global optimum is discussed with the help of terminal constraints, followed by Lyapunov stability of the cost function.

4.1 Terminal Constraints and Convergence of Desired-State

The value of desired-state (χ_i^d) in (17), is based on intermediate-optimum state value ($\tilde{\chi}_i^*$) in (15). For convergence proof, we linearize (15), assuming that the phase difference between the nodes in MG scenario is quite small. DMPSC algorithm employs assumed state (χ_i^a) in (17) for the desired-states, over the complete length of prediction horizon. So, (15) can be written as (24).

To writing (24), in matrix form, representing the complete network, we start with (12),

$$\tilde{F}_i^*(k|t) = \mathbb{Q}_c^{-1}C^{-1}A_cCP(t). \tag{25}$$

Where, $\tilde{F}_i^* = colm\left(\Delta\tilde{f}_i^*\right) \in \mathbb{R}^{n_P\times 1}, C = \mathfrak{D}(c_i) \in \mathbb{R}^{n_P\times n_P}$ and $P = colm(p_i) \in \mathbb{R}^{n_P\times 1}$. Now, (24) in matrix form is presented in (26).

Were, $\acute{P} = colm\left\{\sum_{j\in N_{bP-c,i}}\left(b_{P,ij}v_iv_j\sin\left(\Delta\theta_i(k) - \Delta\theta_j(k)\right)\right)\right\} \in \mathbb{R}^{n_P\times 1}$, $P^L = colm(p_i^L) \in \mathbb{R}^{n_P\times 1}$, $V = \mathfrak{D}(v_i) \in \mathbb{R}^{n_P\times n_P}$, $F = colm(f_i) \in \mathbb{R}^{n_P\times 1}$, $\Delta\theta = colm(\Delta\theta_i) \in \mathbb{R}^{n_P\times 1}$.

Let, $K = \mathbb{Q}_c^{-1}C^{-1}A_cC$ and assuming the voltage at each node to be one per-unit ($V = I$), (26) results in (27).

Remark 3: Hadamard product is used in (27) to divide the neighbouring set N_{bP}. Where, $(A_{bP} \cap A_c) \circ B_P$ represents the neighbouring nodes with power and communication links while, $\acute{P(t)}$ is composed of neighbouring nodes with power link but no communication ($(A_{bP} - A_c) \circ B_P$).

Remark 4: For a matrix $X \in \mathbb{R}^{n\times n}$, $X\mathbb{1}_n$ contains the row sum of X. So, the degree matrix of X can be written as $\mathbb{Q}_X = \mathfrak{D}(X\mathbb{1}_n)$.

Now, let $\mathfrak{B} = (A_c \cap A_{bP}) \circ B_P \in \mathbb{R}^{n_P\times n_P}$, with degree matrix of $\mathfrak{B}$; $\mathbb{Q}_{\mathfrak{B}} = \mathfrak{D}(\mathfrak{B}\mathbb{1}_{n_P}) \in \mathbb{R}^{n_P\times n_P}$. So, (27) becomes,

$$\Delta\tilde{\theta}^*(k|t) = \mathbb{Q}_{\mathfrak{B}}^{-1}\left\{\mathfrak{B}\Delta\theta^a(k|t) + KP(t) - P^L(t) - \acute{P}(t)\right\} \tag{28}$$

Now, we represent $P(t)$, $\acute{P}(t)$ and $P^L(t)$ in terms of assumed phase deviation ($\Delta\theta^a$). From (2) we have,

$$P(t) = \mathfrak{D}\left(\Delta\theta^a(t)\right)B_P\mathbb{1}_{n_P} - B_P\Delta\theta^a(t) + P^L(t),$$
$$P(t) = (\mathbb{Q}_{bP} - B_P)\Delta\theta^a(t) + P^L(t), \tag{29}$$

from (24) and (26) we represent $\acute{P}(t)$ as in (30).

Now, let $\widehat{\mathfrak{B}} = (A_{bP} - A_c) \circ B_P$ and $\widehat{\mathbb{Q}}_{bP} = \widehat{\mathfrak{B}}\mathbb{1}_{n_P}$ so, (30) becomes,

$$\acute{P}(t) = \left(\widehat{\mathbb{Q}}_{bP} - \widehat{\mathfrak{B}}\right)\Delta\theta^a(t), \tag{31}$$

now,

$$P^L(t) = \left(\mathbb{Q}_{bL} - B_L{\mathbb{Q}_{bL}^{\perp}}^{-1}B_L^T\right)\Delta\theta^a(t) + B_L{\mathbb{Q}_{bL}^{\perp}}^{-1}L + P_{LL}, \tag{32}$$

using (29), (31) and (32) in (28) results in (33).

Where, $L = colm\left(p_{l,i}\right) \in \mathbb{R}^{n_L\times 1}$ represents the power consumption by load-nodes. The complete derivation of (32) is available in Appendix I. Note that, (33) is the linearized-matrixed form of (16), represents the intermediate-equilibrium point at a given time instant.

Now, the following lemma defines the equilibrium point of the network in terms of phase deviations.

Lemma 1: For the dynamic system defined in (5), with control objectives (8) and (9), the following is sufficient condition for global optimum point in DMPSC algorithm.

$$\Delta\theta^a(t+1) = \Delta\theta^d(t+1) = \Delta\theta^a(t) = \Delta\theta^d(t). \tag{34}$$

Proof: Considering (17), (34) implies that $\Delta\theta^a(t) = \Delta\theta^d(t) = \Delta\tilde{\theta}^*(t)$ and $\Delta\omega^a(t) = 0$ (for all power-nodes). Now, following the derivation of $\Delta\tilde{\theta}^*(t)$, it means that all power nodes are injecting optimum power and achieved the ELD, at nominal frequency, hence $\chi^a(t) = \chi^*(t)$. ■

Following lemmas, together with Lemma 1, would be useful for convergence proof.

Lemma 2: (Gersgorin Disk Criteria) Let $X = [x_{ij}] \in \mathbb{R}^{n\times n}$ be a matrix, then eigen values (σ_i) of X will lie in union of circles ($\mathcal{C}_i$) defined by,

$$\mathcal{C}_i = \cup_{i=1}^n\{\sigma_i \in \mathbb{C}||\sigma_i - x_{ii}| \le \sum_{j=1,j\neq i}^n x_{ij}\}.$$

$$\sum_{j\in N_{bP\cap c,i}}\left(b_{P,ij}v_iv_j\left(\Delta\tilde{\theta}_i^*(k|t) - \Delta\theta_j^a(k|t)\right)\right) = -\sum_{j\in N_{bP-c,i}}\left(b_{P,ij}v_iv_j\left(\Delta\theta_i(k) - \Delta\theta_j^a(k)\right)\right) - p_i^L(t) + \Delta\tilde{f}_i^*(t), \tag{24}$$

$$\mathfrak{D}\left(\Delta\tilde{\theta}^*(k|t)\right)\{(A_{bP}\cap A_c)\circ VB_PV\mathbb{1}_{n_P}\} - (A_{bP}\cap A_c)\circ VBV\Delta\theta^a(k|t) + \acute{P}(t) + P^L(t) = \mathbb{Q}_c^{-1}C^{-1}A_aCP(t). \tag{26}$$

$$\mathfrak{D}\left(\Delta\tilde{\theta}^*(k|t)\right)\{(A_{bP}\cap A_c)\circ B_P\mathbb{1}_{n_P}\} - \{(A_{bP}\cap A_c)\circ B\}\Delta\theta^a(k|t) = KP(t) - P\acute{}(t) - P^L(t), \tag{27}$$

$$\acute{P}(t) = \mathfrak{D}\left(\Delta\theta^a(t)\right)(A_{bP} - A_c)\circ B_P\mathbb{1}_{n_P} - (A_{bP} - A_c)\circ B_P\Delta\theta^a(t), \tag{30}$$

$$\Delta\tilde{\theta}^*(k|t) = \mathbb{Q}_{\mathfrak{B}}^{-1}\left\{\mathfrak{B}\Delta\theta^a(k|t) + \left\{K(\mathbb{Q}_{bP} - B_P) + \left(K - I_{n_P}\right)\left(\mathbb{Q}_{bL} - B_L{\mathbb{Q}_{bL}^{\perp}}^{-1}B_L^T\right) - \left(\widehat{\mathbb{Q}}_{bP} - \widehat{\mathfrak{B}}\right)\right\}\Delta\theta^a(t) + \left(K - I_{n_P}\right)B_L{\mathbb{Q}_{bL}^{\perp}}^{-1}L + \left(K - I_{n_P}\right)P_{LL}\right\}. \tag{33}$$

$$\Delta\theta^a(\mathcal{N}_p|t+2) = \Delta\theta^d(\mathcal{N}_p|t+1) = (1-\alpha)\Delta\theta^a(\mathcal{N}_p|t+1) + \alpha\Delta\tilde{\theta}^*(\mathcal{N}_p|t+1), \tag{36}$$

$$\Delta\theta^a(\mathcal{N}_p|t+2) = \{(1-\alpha)I_{n_P} + \alpha\mathbb{Q}_{\mathfrak{B}}^{-1}\mathfrak{B}\}\Delta\theta^a(\mathcal{N}_p|t+1) + \alpha\mathbb{Q}_{\mathfrak{B}}^{-1}\{K(\mathbb{Q}_{bP} - B_P) + (K - I_{n_P})(\mathbb{Q}_{bL} - B_L{\mathbb{Q}_{bL}^{\perp}}^{-1}B_L^T) - (\widehat{\mathbb{Q}}_{bP} - \widehat{\mathfrak{B}})\}\Delta\theta^a(t+1) + \alpha\mathbb{Q}_{\mathfrak{B}}^{-1}(K - I_{n_P})\{B_L{\mathbb{Q}_{bL}^{\perp}}^{-1}L + P_{LL}\}, \tag{37}$$

$$\Delta\theta^a(\mathcal{N}_p|t+2) = \mathbb{Z}_1\Delta\theta^a(\mathcal{N}_p|t+1) + \alpha\mathbb{Z}_2\Delta\theta^a(t+1) + \mathbb{Z}_3, \tag{38}$$

$$\Delta\theta^a(\mathcal{N}_p|t+2) = \overline{\mathbb{Z}}_1\Delta\theta^a(\mathcal{N}_p|t+1) + \alpha\overline{\mathbb{Z}}_2\Delta\theta^a(t+1) + \overline{\mathbb{Z}}_3, \tag{39}$$

$$J_i^*(t+1) - J_i^*(t) \le -l_i\left(y_i^{op}(0|t), u_i^{op}(0|t), y_i^a(0|t), y_i^d(0|t)\right) - \sum_{k=0}^{\mathcal{N}_p-1}||y_i^{op} - y_i^a||_S, \qquad i \in N_P. \tag{41}$$

$$J_i^*(t+1) \le J_i\left(y_i^a(:|t+1), u_i^a(:|t+1), y_i^a(:|t+1), y_i^d(:|t+1)\right), \tag{42}$$

$$J_i^*(t+1) \le \sum_{k=0}^{\mathcal{N}_p-1} l_i\left(y_i^a(k|t+1), u_i^a(k|t+1), y_i^a(k|t+1), y_i^d(k|t+1)\right), \tag{43}$$

Lemma 3: The matrix, $\tilde{\mathcal{L}} = [\ell_{ij} \in \mathbb{R}\,|\ell_{ij} \le 0, j \ne i \;\&\; \sum_{j=1,j\ne i}^{n}|\ell_{ij}| = \ell_{ii}], \in \mathbb{R}^{n\times n}$, is an altered Laplacian matrix and $X = \mathfrak{D}(x_{ii}) \in \mathbb{R}^{n\times n}$, with $x_{ii} \in \mathbb{R}_{\ge 0}$, then $\tilde{\mathcal{L}} + X$ is invertible if at least one $x_{ii} > 0$.

Proof: The proof of the lemma is similar to the one used for sum of Laplacian and pinning matrix in [30]. ■

Theorem 1: If $\mathbb{G}$ satisfies Assumption 1, then terminal state of problem $\mathbb{F}_i$ converges asymptotically to equilibrium state, satisfying the objectives (8) and (9).

Proof: Constrained by (18) and (19), the χ_i^p, reaches χ_i^d at the end of prediction horizon. Considering (21), the assumed value of output can be written as,

$$y_i^a(\mathcal{N}_p - 1|t+1) = y_i^p(\mathcal{N}_p|t) = y_i^d(\mathcal{N}_p|t). \tag{35}$$

Since, $\Delta\omega_i^a(\mathcal{N}_p - 1|t+1) = \Delta\omega_i^p(\mathcal{N}_p|t) = 0$, so $\Delta\theta_i^a(\mathcal{N}_p|t+1) = \Delta\theta_i^d(\mathcal{N}_p|t)$. Now, the terminal value of desired phase deviation for next iteration is given by (36).

Using (33) in (36) results in (37).

Let, $Z_1 = \alpha\mathbb{Q}_{\mathfrak{B}}^{-1}\mathfrak{B}, \in \mathbb{R}^{n_P\times n_P}$, $\mathbb{Z}_1 = (1-\alpha)I_{n_P} + Z_1, \in \mathbb{R}^{n_P\times n_P}$, $\mathbb{Z}_2 = \mathbb{Q}_{\mathfrak{B}}^{-1}\left(K(\mathbb{Q}_{bP} - B_P) + (K - I_{n_P})\left(\mathbb{Q}_{bL} - B_L{\mathbb{Q}_{bL}^{\perp}}^{-1}B_L^T\right) - \left(\widehat{\mathbb{Q}}_{bP} - \widehat{\mathfrak{B}}\right)\right), \in \mathbb{R}^{n_P\times n_P}$ and $\mathbb{Z}_3 = \alpha\mathbb{Q}_{\mathfrak{B}}^{-1}(K - I_{n_P})\left(B_L{\mathbb{Q}_{bL}^{\perp}}^{-1}L + P_{LL}\right), \in \mathbb{R}^{n_P\times 1}$. So, (37) becomes (38).

From (16), we have $\Delta\tilde{\theta}_1^*(k) = 0$, so we replace the first rows of Z_1 in (38) with zero. Let $\overline{\mathbb{Z}} = \mathfrak{D}([0\ 1\ 1\ \dots\ 1]^T) \in \mathbb{R}^{n_P\times n_P}$. Now, let $\overline{\mathbb{Z}}_1 = (1-\alpha)\mathrm{I}_{n_P} + \overline{\mathbb{Z}}Z_1, \in \mathbb{R}^{n_P\times n_P}$, $\overline{\mathbb{Z}}_2 = \overline{\mathbb{Z}}\mathbb{Z}_2, \in \mathbb{R}^{n_P\times n_P}$ and $\overline{\mathbb{Z}}_3 = \overline{\mathbb{Z}}\mathbb{Z}_3, \in \mathbb{R}^{n_P\times 1}$. So, (38) results in (39).

Lemma 4: The eigen values ($\lambda_{1,i}$) of $\overline{\mathbb{Z}}_1$ lies within the unit circle for all values of $\alpha \in (0,1)$.

Proof: All the diagonal values of $\overline{\mathbb{Z}}_1$ are equal to $(1-\alpha)$, while the row sum of $\overline{\mathbb{Z}}_1$ is equal to α, except the first row. So according to lemma 2, all the eigen values of $\overline{\mathbb{Z}}_1$ lies within the union of following disks, $\{|\lambda_{1,i} - (1-\alpha)| \le 0\} \cup \{|\lambda_{1,i} - (1-\alpha)| \le \alpha\}$ or $\{1 - 2\alpha \le \lambda_{1,i} \le 1\}$, for $i = 1, \dots, n_P$.

Now, we prove using contradiction that eigen values of $\overline{\mathbb{Z}}_1$ does not lies on boundary of unit circle. Let, some eigen values of $\overline{\mathbb{Z}}_1$ lie on boundary of unit circle ($\lambda_{1,i}$=1) and let, ρ be the corresponding eigen vector, then we can write,

$$\overline{\mathbb{Z}}_1\,\rho = \rho,$$
$$\left((1-\alpha)I_{n_P} + \alpha\overline{\mathbb{Z}}\mathbb{Q}_{\mathfrak{B}}^{-1}\,\mathfrak{B}\right)\rho = \rho,$$
$$\alpha\left(I_{n_P} - \overline{\mathbb{Z}}\mathbb{Q}_{\mathfrak{B}}^{-1}\,\mathfrak{B}\right)\rho = 0.$$

Since, $\alpha \ne 0$, now it remains to prove that, $\Gamma^{n_P} = I_{n_P} - \overline{\mathbb{Z}}\mathbb{Q}_{\mathfrak{B}}^{-1}\,\mathfrak{B} \in \mathbb{R}^{n_P\times n_P}$ is positive definite. Since, the top row of Γ^{n_P} contains zeros except the first element which is 1, we can remove the top row and first column of Γ^{n_P} without effecting its determinant. Now, we can represent the remaining matrix $\Gamma^{n_P-1} = \left(I_{n_P-1} - \mathbb{Q}_{\mathfrak{B}}^{-1}\,\mathfrak{B}\right) \in \mathbb{R}^{n_P-1\times n_P-1}$, by modified Laplacian matrix $\tilde{\mathcal{L}} \in \mathbb{R}^{(n_P-1)\times(n_P-1)}$.

$$\Gamma^{n_P-1} = \left(I_{n_P-1} - \mathbb{Q}_{\mathfrak{B}}^{-1}\,\mathfrak{B} - \Psi\right) + \Psi = \tilde{\mathcal{L}} + \Psi.$$

Where, $\tilde{\mathcal{L}} = \left(I_{n_P} - \mathbb{Q}_{\mathfrak{B}}^{-1}\,\mathfrak{B} - \Psi\right)$, $\Psi = \mathfrak{D}(\psi_{j1}) \in \mathbb{R}^{(n_P-1)\times(n_P-1)}, j = 2, \dots, n_P$ and $\psi_{ij} \in \mathbb{R}_{\ge 0}$ are the elements of Γ^{n_P}. Since, $\mathbb{G}$ forms a connected graph, Ψ cannot be completely zero and from lemma 3, $\tilde{\mathcal{L}} + \Psi$ is positive definite, completing the proof of lemma 4. ■

The eigen values ($\lambda_{2,i}$) of $\overline{\mathbb{Z}}_2$ however, may lies outside the unit circle. With proper selection of step size α, the eigen values can be forced to lie inside the unit circle. Let, the maximum eigen value of $\overline{\mathbb{Z}}_2$ be $\lambda_{2,max}$, and with $\alpha < \lambda_{2,max}^{-1}$, then eigen values of $\alpha\overline{\mathbb{Z}}_2$ will lie within unit circle.

The eigen values of $\overline{\mathbb{Z}}_1$ and $\alpha\overline{\mathbb{Z}}_2$ show the asymptotic converge of (38) to steady state, whereupon satisfies lemma 1, completing the proof of Theorem 1. ■

Remark 5: Smaller values of α will move the eigen values of $\overline{\mathbb{Z}}_2$ towards the origin. On the other hand, eigen values of $\overline{\mathbb{Z}}_1$ lies between $(1-2\alpha) < \lambda_i < 1$. The small values of α will push the eigen values of $\overline{\mathbb{Z}}_1$ towards the boundary, resulting in slow convergence. So, the optimum value of α does not lie near the boundaries of interval $(0,1)$, but somewhere in the middle.

4.2 Convergence of Cost Function

Assuming, that the system satisfies Theorem 1 at time $t = \boldsymbol{t}$ ($\boldsymbol{t} \in \mathbb{R}_{>0}$) then, $y_i^p(\mathcal{N}_p|\boldsymbol{t}) = y_i^*(\mathcal{N}_p|\boldsymbol{t})$, then at any time $t \ge \boldsymbol{t}$, a feasible solution of problem $\mathbb{F}_i$ is given by [29],

$$\left(y_i^p(:|t), u_i^p(:|t)\right) = \left(y_i^a(:|t), u_i^a(:|t)\right). \tag{40}$$

$$J_i^*(t+1) \le \sum_{k=0}^{\mathcal{N}_p-2} l_i\big(y_i^{op}(k+1|t), u_i^{op}(k+1|t), y_i^{op}(k+1|t), y_i^d(k+1|t)\big), \tag{45}$$

$$J_i^*(t+1) \le \sum_{k=1}^{\mathcal{N}_p-1} l_i\big(y_i^{op}(k|t), u_i^{op}(k|t), y_i^{op}(k|t), y_i^d(k|t)\big), \tag{46}$$

$$J_i^*(t+1) - J_i^*(t) \le \sum_{k=1}^{\mathcal{N}_p-1} l_i\big(y_i^{op}(k|t), u_i^{op}(k|t), y_i^{op}(k|t), y_i^d(k|t)\big) - \sum_{k=0}^{\mathcal{N}_p-1} l_i\big(y_i^{op}(k|t), u_i^{op}(k|t), y_i^a(k|t), y_i^d(k|t)\big), \tag{47}$$

$$\le \sum_{k=1}^{\mathcal{N}_p-1}\big(||y_i^{op}(k|t) - y_i^d(k|t)||_R + ||y_i^{op}(k|t) - y_i^{op}(k|t)||_S\big) - \sum_{k=0}^{\mathcal{N}_p-1}\big(||y_i^{op}(k|t) - y_i^d(k|t)||_R + ||y_i^{op}(k|t) - y_i^a(k|t)||_S\big), \tag{48}$$

$$\le -l_i\left(y_i^{op}(0|t), u_i^{op}(0|t), y_i^a(0|t)\right) - \sum_{k=0}^{\mathcal{N}_p-1} ||y_i^{op} - y_i^a||_S. \tag{49}$$

$$\mathbb{J}^*(t+1) - \mathbb{J}^*(t) \le -\sum_{i=1}^{N_P} l_i\left(y_i^{op}(0|t), u_i^{op}(0|t), y_i^a(0|t), y_i^d(0|t)\right) - \sum_{i=1}^{N_P}\sum_{k=0}^{\mathcal{N}_p-1} ||y_i^{op} - y_i^a||_S, \tag{50}$$

(40) provides a feasible but not necessarily an optimal solution for $\mathbb{F}_i$. Now, the optimum value of the cost function is given by, $J_i^*(t) = J_i^*\big(y_i^{op}(:|t), u_i^{op}(:|t), y_i^a(:|t), y_i^d(:|t)\big)$.

Theorem 2: If $\mathbb{G}$ satisfy Assumption 1 and Theorem 1, then local cost function converges asymptotically and satisfies (41).

Proof: We start by comparing a sub-optimal cost function using (40), with the optimum cost function (J_i^*), at time $t+1 > \boldsymbol{t}$, as shown in (42) and (43).

Considering, (18), (20) and (40); $l_i\big(y_i^a(\mathcal{N}_p - 1|t+1), u_i^a(\mathcal{N}_p - 1|t+1), y_i^a(\mathcal{N}_p - 1|t+1), y_i^d(\mathcal{N}_p - 1|t+1)\big) = 0$. Now, from (21); $y_i^a(k|t+1) = y_i^{op}(k+1|t)$ so (43) results in (45).

Now, changing the index of summation in (45) provides (46), then subtracting $J_i^*(t)$ from $J_i^*(t+1)$, results in (47), (48) and (49).

From definition of cost function (20); $\left(l_i\big(y_i^{op}(0|t), u_i^{op}(0|t), y_i^a(0|t), y_i^d(0|t)\big) + \sum_{k=0}^{\mathcal{N}_p-1} ||y_i^{op} - y_i^a||_S\right) \ge 0$, satisfying Theorem 2. ■

Theorem 3: If $\mathbb{G}$ satisfy Assumption 1, Theorem 1&2, then total cost of network converges asymptotically and satisfies (50).

Where $\mathbb{J}^*(t) = \sum_{i=1}^{N_P} J_i^*(t)$.

Proof: The proof of Theorem 3 is fairly, obvious; by summing (49) for all power-nodes gives (50). ■

5. Performance Validation

To evaluate the performance of proposed DMPSC, a MATLAB based experimental setup is established consists of five power-nodes; $N_P = \{n_1, \dots n_5\}$, with local-loads; $P_{LL} = \{0, 0, 0, p_{LL,4}, 0\}$ and two load-node $N_L = \{n_6, n_7\}$, as shown in Figure 1. The power lines connecting the nodes are purely inductive. The parameters of power-nodes and susceptance matrices B_P and B_L are represented in Appendix II. The parameters of DMPSC (and DAI), and adjacency matrix A_c associated with the communication links are also listed in Appendix II. For comparative analysis, DAI based SC is also tested for same experimental setup. Keeping in view, the slow response of DAI, the simulation time is set to "40 seconds".

5.1 Test Case

Two different types of disturbances; abrupt change in incremental cost (c_i) and load ($p_{l,i}$), are introduced to test the performance of DMPSC. The simulation of time "7.5 seconds" is assumed to be the start of peak-hour where, the incremental cost of four (out of five) nodes is increased abruptly. Then, instant load change is introduced at simulation time of "15 seconds", resulting in power and frequency fluctuations. The change in incremental cost is a planned-disturbance where the start of peak hours is known in advance to every node and each node communicates its incremental cost in the prediction horizon, to its neighbouring nodes. However, sudden load change introduced at "15 seconds" is an unplanned-disturbance where power-nodes do not have prior knowledge of the disturbance. Table A2 and Table A3 in Appendix II, lists the values of incremental costs and load demands before and after the respective disturbances.

The simulations are performed at two separate sampling times, which corresponds to different communication-bandwidths in physical implementation, while keeping the rest of the environment identical. First, the simulation is performed with sampling time equal to 10ms, then sampling time is increased to 100ms, indicating a reduction in bandwidth. Figure 2 and Figure 3 represent the simulation results of DMPSC and DAI with sampling time equal to 10ms, respectively, while Figure 4 and Figure 5 contain the respective results at 100ms sampling time.

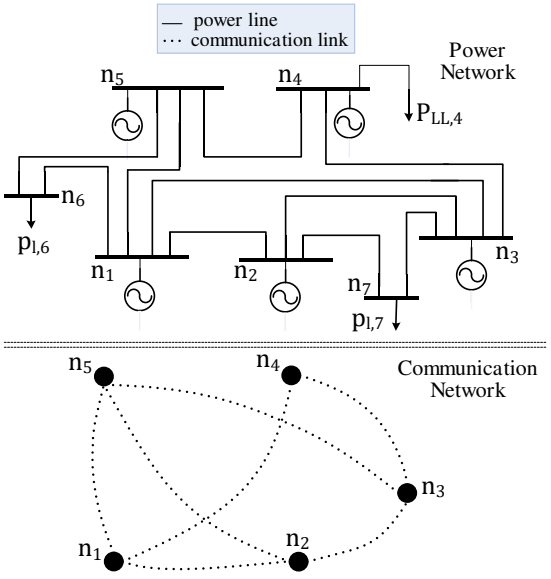

Figure 1: 7-node MG Model.

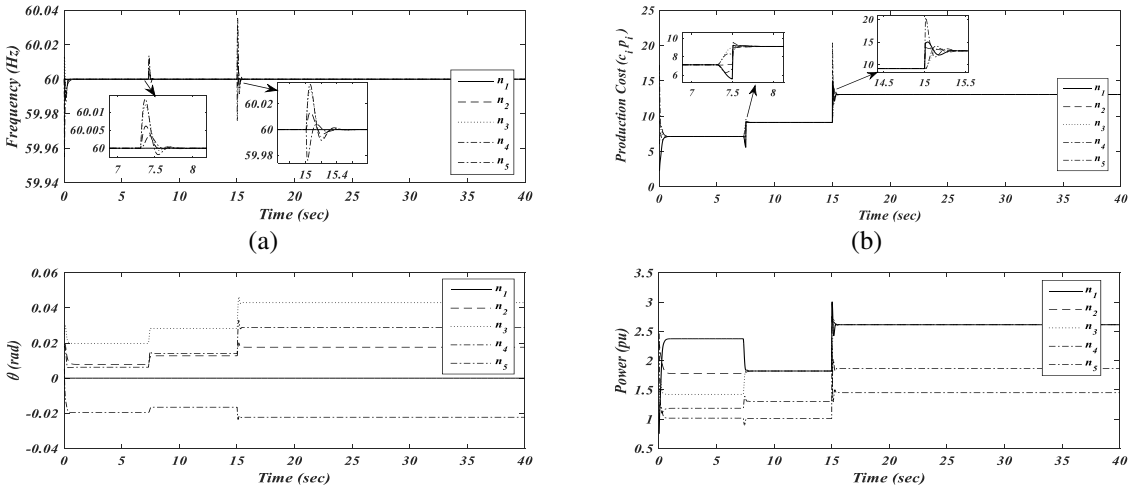

(a) (b)

(c) (d)

Figure 2: Simulation results of DMPSC (sampling time: 10ms).

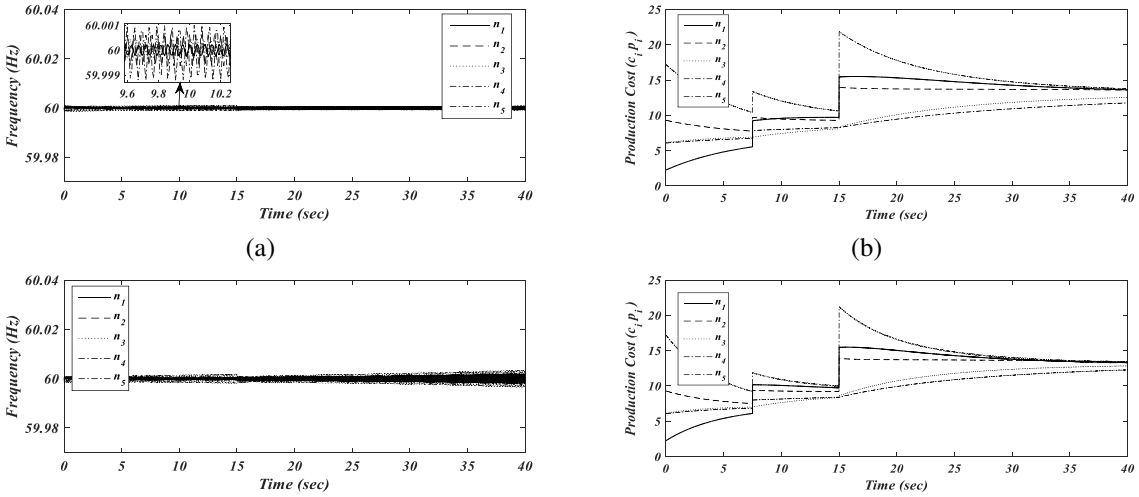

(a) (b)

(c) (d)

Figure 3: Simulation results of DAI (sampling time: 10ms).

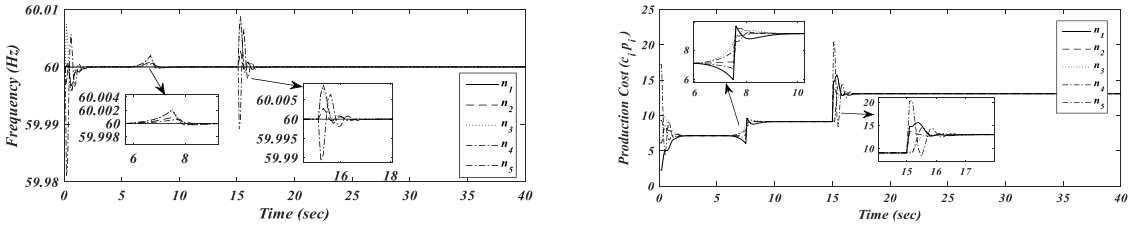

(a) (b)

Figure 4: Simulation results of DMPSC (sampling time: 100ms).

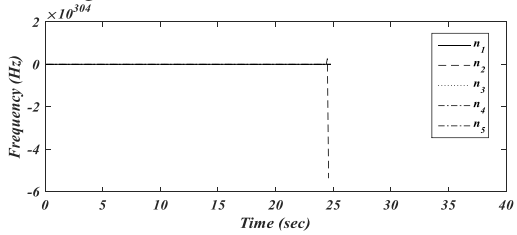

Figure 5: Simulation results of DAI (sampling time: 100ms).

5.2 Simulation Results for DMPSC (Sampling Time: 10ms)

The deviation in frequencies in response to the induced disturbances is illustrated in Figure 2a. The frequency deviation in response to planned-disturbance at 7.5 seconds, is much smaller as compared to deviation produced due to unplanned-disturbance at 15 seconds. In case of planned disturbance, each node starts anticipating the upcoming change before 7.5 seconds, resulting in relatively smooth transition. However, in both the cases the frequency

is restored back to its nominal value within 0.5 seconds. The Figure 2b represents the convergence of power-nodes to identical cost, to achieve the ELD. Both the disturbances result in increased identical cost ($c_i p_i$), first due to increase in incremental cost, followed by the increase in power demand. The Figure 2c represents the phase deviation of individual nodes. The phase of the first node is forced to zero, to keep minimum phase difference between MG and main grid at PCC. In Figure 2d the power injection profiles of each power-node settle rapidly an optimum value after each disturbance.

5.3 Simulation Results for DAI (Sampling Time 10ms)

The performance of DAI is presented in Figure 3. The system fails to converge to identical cost even at simulation time of "40 seconds". The DAI manifests active frequency regulation, but possesses sustained small-scale oscillations as illustrated in Figure 3a. The convergences of DAI is achieved with gain-value; $k_w = 8 \times 10^4$ and $k_p = 6$, in control law equation (10). The values of $k_w > 8 \times 10^4$, may reduce the magnitude of oscillations but at the expense of even slower convergence to identical cost. The convergence to identical cost is shown in Figure 3b. The slow response in Figure 3b may be attributed to small value of k_p however, increasing k_p drastically affects the frequency regulation. Figure 3c and Figure 3d represent the frequency regulation and convergence to identical cost for k_w and k_p equal to 8×10^4 and 7 respectively. Figure 3d represents improved convergence rate as compared to Figure 3b while on the other hand, Figure 3c shows divergent behavior in frequency. The Figure shows increased oscillations in frequency, which increases in magnitude with time.

5.4 Simulation Results DMPSC and DAI (Sampling Time: 100ms)

The results of DMPSC in Figure 4 illustrate relatively less overshoot but longer convergence time, compared to Figure 2. The steady-state is achieved within 2 seconds for both the planned and unplanned disturbances. Figure 4a and Figure 4b represents the achievement of control objectives (8) and (9) respectively. The increased sampling time resulted in slightly increased convergence time. DAI on the other hand, failed to attain the stability. Figure 5 shows the results for DAI ($k_w = 8 \times 10^4$ and $k_p = 6$), illustrating divergence in frequency.

The simulation results affirm that proposed DMPSC has fast and robust convergence to steady state after subjection to planned and unplanned, abrupt changes. Benefiting from inherent capability of MPC to anticipate the future disturbances, the results illustrate minimal fluctuations in the power and frequency in response to planned disturbances. Both DMPSC and DAI demonstrate efficient frequency regulation, the magnitude of frequency deviation is negligible in response to significant disturbances in system, that can be attributed to the absence of physical rotational inertia in the system. DAI however, requires a significant amount of time to achieve ELD as compared to DMPSC. Lastly, DMPSC also has the capability to operate at much smaller bandwidth than DAI.

6. Conclusion

The paper proposes distributed model predictive based secondary control for frequency regulation, economic load dispatch and phase synchronization of islanded microgrid. The proposed control benefits from inherent capabilities of distributed model predictive control including, anticipation of upcoming changes/fluctuations in the system and fast response. The control algorithm is implemented locally at each power-node in the network so, the size of the network does not affect the computational complexity in the system. Due to absence of physical rotational inertia, the control provides active frequency regulation. However, unlike contemporary secondary control schemes, the control provides rapid convergence to identical-cost, forcing the power-nodes to inject optimum power in the system. The control also ensures minimum phase difference between microgrid and main grid, at point of common coupling. The proposed control outperforms the DAI in terms of fast convergence to equilibrium point and ability to operate at low bandwidth. The paper also presents sufficient condition for convergence and proves asymptotic stability of the system using sum of cost functions as Lyapunov candidate function.

The future research openings related to the presented work contain; using the more generalized network topology and mechanism to cater the variations in network topology and parameters. The problems related to communication among the nodes is also an important issued that need to be addressed.

References

[1] M. S. Mahmoud, M. S. Rehman, F. M. A. L. Sunni, "Review of microgrid architecture – a system of systems perspective", IET Renewable Power Generation, vol. 9, issue 8, 2015.

[2] R. Zamora, A.K. Srivastava, "Multi-Layer Architecture for Voltage and Frequency Control in Networked Microgrids", IEEE Transactions on Smart Grid, vol: 9, issue 3, 2018, doi:10.1109/TSG.2016.2606460.

[3] Xiaoqing Lu, N. Chen, Y Wang, Liang Qu, "Distributed impulsive control for islanded microgrids with variable communication delays", IET Control Theory & Applications, 2016 doi: 10.1109/PSC.2016.7462854.

[4] Olve Mo, S. D'Arco, J.A. Suul, "Evaluation of Virtual Synchronous Machines With Dynamic or Quasi-Stationary Machine Models" IEEE Transaction on Industrial Electronics, vol. 64, issue. 7, 2017, doi: 10.1109/TIE.2016.2638810

[5] F. Dorfler, J. W. Simpson-Porce, F. Bullo, "Breaking the Hierarchy: Distributed Control & Economic Optimality in Microgrids" IEEE Transaction on Control of Network System, vol.3, issue. 3, 2016, doi: 10.1109/TCNS.2015.2459391.

[6] Kaihua Xi, Johan L.A, Dubbeldam, "Power-Imbalance Allocation Control of Power Systems-Secondary Frequency Control", Automatica, 92(2018), 72-85, doi: 10.1016/j.automatica.2018.02.019.

[7] Trip, Sebastian, Burger, "An internal model approach to (optimal) frequency regulation in power grids with time-varying voltages", Automatica, 64(2016), 240-253.

[8] Li, Na, Chen, Lijun, "Connecting automatic generation control and economic dispatch from an optimization view" American control conference (pp. 735-740), 2014.

[9] Tine L. Vandoorn, B. Meersman, "Transition From Islanded to Grid-Connected Mode of Microgrid with Voltage Based Droop Control*" IEEE Transaction on* Power Systems, vol. 28, issue. 3, 2013.

[10] William C., Edwards, S. Manson, "Microgrid islanding and grid restoration with off-the-shell utility protection equipment" IEEE Canada International Humanitarian Technology Conference (IHTC), 2017, doi: 10.1109/IHTC.2017.8058185

[11] IEEE Standard 1547-2003, IEEE Standard for Interconnecting Distributed Resources With Electric Power Systems.

[12] Josep M., Guerrero, Juan C., "Hierarchical Control of Droop-Controlled AC and DC Microgrids – A General Approach Towards Standardization", IEEE Transaction on Industrial Electronics, vol. 58, issue, 1, 2011, doi: 10.1109/TIE.2010.2066534

[13] Zhao, J., Dorfler F., "Distributed control and optimization in DC microgrids", Automatica, 61(2015), 18 – 26.

[14] Zaheeruddin, M. Manas, "Renewable energy management through microgrid central controller design: An approach to integrate solar, wind and biomass with battery", Energy Report, 1(2015) 156 – 163.

[15] A. G. Tsikalakis, N. D. Hatziargyriou, "Centralized Control for Optimizing Microgrids Operation", IEEE Transactions on Energy Conversion, vol. 23, issue. 1, 2008.

[16] A. Tuckey, S. Sabihi, S. Round, "Decentralized control of a microgrid", European Control Conference on Power Electronics and Applications, 2017, doi: 10.23919/EPE17ECCEEurope.2017.8098969

[17] N. Cai, J. Mitra, "A decentralized control arechitecture for microgrid with power electronic interfaces", IEEE North American Power Symposium, 2010, doi: 10.1109/NAPS.2010.5619963

[18] G. Lou, W. Gu, L. Wang, Bin Xu, Ming Wu, W. Sheng, "Decentralised secondary voltage and frequency control scheme for islanded microgrid based on adaptive state estimator" IET Generation, Transmission & Distribution, vol. 11, issue 15, 2017.

[19] C. Zhao, E. Mallada, F. Dorfler, "Distributed Frequency Control for Stability and Economic Dispatch in Power Networks", American Control Conference, 2015.

[20] L.Y. Lu, H. J. Liu, H. Zhu, "Distributed secondary control for isolated microgrid under malicious attacks", North American Power Symposium (NAPS), 2016, doi: 10.1109/NAPS.2016.7747929

[21] Ji Xiang, Yu Wang, Yanjun Li, Wei We, "Stability and steady-state analysis of distributed cooperative droop controlled DC microgrids", IET Control Theory & Applications, 2016.

[22] A. J. Wood, B. F. Wollenberg, Power Generation, Operation and Control, John Wiley & Sons, 2005.

[23] F. Dorfler, S. Grammatico, "Gather-and-broadcast frequency control in power systems", Automatica 79(2017) 296 – 305.

[24] Andreasson, Dimarogonas, Sandberg, "Distributed PI-control with applications to power systems frequency control", American Control Conference, 2014, (pp. 3183 – 3188).

[25] X. Wu, C. Shen, "Distributed optimal control for stability enhancement of microgrids with multiple distributed generators", IEEE Transactions on Power Systems, vol. 2, issue. 5, 2017, doi: 10.1109/TPWRS.2017.2651412.

[26] J. Schiffer, F. Dorfler, E. Fridman, "Robustness of distributed averaging control in power systems: Time delays & dynamic communication topoloty", Automatica, 80(2017), 261 – 271.

[27] C. Ahumada, R. Cárdenas, D. Sáez, "Secondary Control Strategies for Frequency Restoration in Islanded Microgrids With Consideration of Communication Delays" IEEE Transactions on SMART GRID, vol. 7, No. 3, 2016.

[28] Y. Zheng, S. Eben Li, K. Li, F. Borrelli, "Distributed Model Predictive Control for Heterogenous Vehicle Platoons under Unidirectional Topologies", IEEE Transactions on Control Systems Technology vol. 25 , Issue. 3, 2017.

[29] W. Dunbar and D. Caveney, "Distributed receding horizon control of vehicle platoons: Stability and string stability," IEEE Trans. Autom. Control, vol. 57, no. 3, 2012.

[30] Y. Wu, S. Eben Li, Y. Zheng, "Distirbuted Sliding Mode Control for Multi-vehicle Systems with Positive Definite Topology", IEEE 55th Conference on Decision and Control (CDC), USA, 2016.

Appendix I

From (2), (3) and linearization of (4), the power supplied by i^{th} power node to load nodes is given by,

$$p_{Li}(t) = \sum_{j\in N_{bL,i}}\left(b_{L,ij}v_i v_j\left(\Delta\theta_i^a(t) - \Delta\theta_j(t)\right)\right) + p_{LLi}, \quad i \in N_P, \tag{a1}$$

Writing (a1) for whole network and using value of voltage to be $1(pu)$,

$$P^L(t) = \mathfrak{D}\left(\Delta\theta^a(t)\right)\left(B_L\mathbb{1}_{n_L}\right) - B_L\Delta\theta^{(j)}(t) + P_{LL},$$

$$P^L = \mathbb{Q}_{bL}\Delta\theta^a(t) - B_L\Delta\theta^{(j)}(t) + P_{LL}, \tag{a2}$$

Where, $\Delta\theta^{(j)} = colm(\Delta\theta_j) \in \mathbb{R}^{n_L \times 1}$, $j \in N_L$ represents the phase deviation of load-node. Now, the power absorbed by j^{th} load-node is given by,

$$p_{l,j}(t) = \sum_{i=1}^{N_P} \left(b_{L,ij} \left(\Delta\theta_i^a(t) - \Delta\theta_j(t) \right) \right), \quad j \in N_L, \qquad \text{(a3)}$$

Writing (a3) for complete network,

$$L = B_L^T \Delta\theta^a(t) - \mathfrak{D}\left(\Delta\theta^{(j)}(t)\right)\left(B_L^T \mathbb{1}_{n_P}\right),$$
$$L = B_L^T \Delta\theta^a(t) - \mathbb{Q}_{bL}^{\perp}\theta^{(j)}(t),$$
$$\theta^{(j)}(t) = {\mathbb{Q}_{bL}^{\perp}}^{-1} B_L^T \Delta\theta^a(t) - {\mathbb{Q}_{bL}^{\perp}}^{-1} L, \qquad \text{(a4)}$$

Using (a4) in (a2)

$$P^L = \mathbb{Q}_{bL}\Delta\theta^a(t) - B_L\left({\mathbb{Q}_{bL}^{\perp}}^{-1} B_L^T \Delta\theta^a(t) - {\mathbb{Q}_{bL}^{\perp}}^{-1} L\right) + P_{LL},$$
$$P^L = \left(\mathbb{Q}_{bL} - B_L {\mathbb{Q}_{bL}^{\perp}}^{-1} B_L^T\right)\Delta\theta^a(t) + B_L {\mathbb{Q}_{bL}^{\perp}}^{-1} L + P_{LL}, \quad \text{(a5)}$$

Appendix II

Table A1 Power-nodes parameters

Power-nodes	m(pu)	$d(pu)$
n_1	5.22	1.60
n_2	3.98	1.22
n_3	4.49	1.38
n_4	4.22	1.42
n_5	5.4	1.30

Table A2 Incremental Cost

Power-nodes	Incremental Cost (before 1.5 sec), (pu)	Incremental Cost (after 1.5 sec), (pu)
n_1	3	5
n_2	4	5
n_3	5	5
n_4	6	7
n_5	7	9

Table A3 Load-nodes Power

Load-nodes	Load (pu) (Before 3 seconds)	Load (pu) After 3 seconds
n_6	4.956	7.352
n_7	1.99	2.970

Table A4 Initial States

Power-nodes	$\Delta\theta_{o,i}$ (rad)	$\Delta\omega_{o,i}$ (rad/sec)	$\Delta f_{o,i} = u_{o,i}$
n_1	0	0	1
n_2	0.0191	0	1
n_3	0.0251	0	1
n_4	0.0183	0	1
n_5	0.0053	0	1

Adjacency Matrix: $A_c = \begin{bmatrix} 0 & 1 & 0 & 1 & 1 \\ 1 & 0 & 1 & 0 & 1 \\ 0 & 1 & 0 & 1 & 1 \\ 1 & 0 & 1 & 0 & 0 \\ 1 & 1 & 1 & 0 & 0 \end{bmatrix}$.

Local load (pu): $P_{LL} = \{0 \quad 0 \quad 0 \quad 0.833 \quad 0\}$.

Susceptance Matrices:

$$B_P = \begin{bmatrix} 0 & -32.34 & -30.76 & 0 & -30.99 \\ -32.34 & 0 & -29.38 & 0 & 0 \\ -30.76 & -29.38 & 0 & -25.85 & 0 \\ 0 & 0 & -25.85 & 0 & -27.34 \\ -30.99 & 0 & 0 & -27.34 & 0 \end{bmatrix}$$

$$B_L = \begin{bmatrix} -25.45 & 0 \\ 0 & -28.16 \\ 0 & -1.473 \\ 0 & 0 \\ -27.63 & 0 \end{bmatrix}.$$

DMPSC Parameters: $R = \begin{bmatrix} 100 & 0 \\ 0 & 10 \end{bmatrix}$, $S = \begin{bmatrix} 1 & 0 \\ 0 & 1 \end{bmatrix}$, $\alpha = 0.8$.

DAI parameters: $k_w = 8 \times 10^4$, $k_p = 6$.